Level structure in ^{143}Nd

X. H. Zhou,[1,2] H. Tsuchida,[3] Y. Gono,[3] A. Odahara,[4] E. Ideguchi,[2] T. Morikawa,[3] M. Shibata,[3] H. Watanabe,[3] M. Miyake,[3]
T. Tsutsumi,[3] S. Motomura,[3] T. Kishida,[2] S. Mitarai,[3] and M. Ishihara[2]

[1]*Institute of Modern Physics, Chinese Academy of Sciences, Lanzhou 730000, China*
[2]*RIKEN, Hirosawa 2-1, Wako, Saitama 351-01, Japan*
[3]*Department of Physics, Kyushu University, Hakozaki 6-10-1, Fukuoka 812, Japan*
[4]*Nishinippon Institute of Technology, Kanda, Fukuoka 800-03, Japan*
(Received 12 May 1999; published 15 December 1999)

The high-spin states of ^{143}Nd have been studied in the ^{130}Te(^{18}O,$5n$)^{143}Nd reaction at a beam energy of 80 MeV using techniques of in-beam γ-ray spectroscopy. Measurements of γ-γ-t coincidences, γ-ray angular distributions, and γ-ray linear polarizations were performed. A level scheme of ^{143}Nd with spin and parity assignments up to $53/2^+$ is proposed, including a high-lying isomer with a measured half-life of 35 ± 8 ns. While a weak coupling model can explain the level structure up to the $J^{\pi} = 39/2^-$ state, this model cannot reproduce the higher-lying states. The characteristics of the high-spin isomer, as well as the level structure in ^{143}Nd, were also stressed with a deformed independent particle model.

PACS number(s): 23.20.Lv, 21.60.Cs, 27.60.+j

I. INTRODUCTION

Many odd-A nuclei near $Z=64$, $N=82$ exhibit a level structure with spin sequences and energy spacings similar to those of the yrast level scheme of adjacent even-even nuclei. This is particularly true of the $N=83$ isotones, which have been proved to be good examples of weak coupling between the unpaired valence neutrons and the even-even spherical core nucleus [1–4]. High-spin yrast states in the $N=82$, doubly even nuclei are generated primarily by excitations of their valence protons [5,6]. The additional valence neutron of the $N=83$ nucleus couples weakly with the core excitation [1–4]. In the present work, we report a much revised level scheme for ^{143}Nd with spin and parity assignments up to the state at 10 132 keV, leading to a more complete understanding of the weak coupling behavior along the yrast line in ^{143}Nd.

High-spin isomers were observed systematically in the $N=83$ isotones with proton number Z from 68 to 61 [7–15]. The characteristics of these high-spin isomers can be well described in the framework of a deformed independent particle model (DIPM) [16], which deals with independent particle configurations in an axially symmetric deformed potential. The single particle energies at zero deformation were deduced from the experimental data [16]. The DIPM calculations assigned the isomers to be of the stretched configurations $[\nu(f_{7/2}h_{9/2}i_{13/2})\pi(h^2_{11/2})]^+_{49/2}$ and $[\nu(f_{7/2}h_{9/2}i_{13/2})\pi(d^{-1}_{5/2}h^2_{11/2})]^+_{27}$ in the odd-A and odd-odd $N=83$ isotones, respectively [15]. These configurations may induce oblate deformations, while the lower-spin states have near spherical shapes [15]. Therefore, the high-spin isomers in the $N=83$ isotones were interpreted to be caused by sudden changes in nuclear shape, which was confirmed by the deformation parameters of the yrast isomers in ^{147}Gd, deduced from experimental quadrupole moments [17,18]. One goal of the present investigation is to search for the corresponding high-spin isomer in ^{143}Nd. The level structure of ^{143}Nd was studied in previous works [4,19–21], but no high-spin isomer has been reported so far.

In nuclei with spherical or near spherical shapes, high-spin states are generally formed by excitations of valence nucleons. The higher spin states require more nucleons to provide the angular momentum, increasing the possibility of the nucleons aligning their angular momenta along an axis, so it would be expected that aligned, or almost aligned configurations dominate the yrast lines in the high-spin region [16]. Thus, the deformed independent particle model [16], which was made to treat aligned configurations, should best describe the high-lying level structure in nuclei with a small deformation.

II. EXPERIMENTAL TECHNIQUES AND RESULTS

The excited states in ^{143}Nd were populated using the ^{130}Te(^{18}O,$5n$)^{143}Nd reaction at a beam energy of 80 MeV. This beam energy was chosen because it was demonstrated, from previous studies of high-spin states in ^{143}Nd, that this nucleus had a favorable yield near this energy [4,19–21]. Measurements of γ-γ coincidences, γ-ray angular distributions, and γ-ray linear polarizations were performed.

For the γ-γ coincidence experiment, a 1.8 mg/cm^2 target of isotopically enriched ^{130}Te, evaporated onto a 2.8 mg/cm^2 aluminum backing, was used. The pulsed ^{18}O beam with a time repetition of 51 ns was provided by the cyclotron at the KEK Tanashi/CNS. γ-γ-t data were accumulated with five BGO(AC)HP Ge detectors, having energy resolutions of 1.9–2.3 keV at 1.33 MeV. Here, t refers to the relative time difference between any two coincident γ rays detected within ± 1000 ns. A total of 70×10^6 coincidence events were recorded event by event for off-line analysis. After accurate gain matching, the γ-γ coincidence data were sorted off-line into three $4K \times 4K$ matrices under three different coincidence time conditions. From these matrices coincidence spectra gated on specific γ-ray peaks were produced, and the resulting spectra were then grouped in terms of three coincidence time ranges: (1) -450 ns$\leqslant t$ $\leqslant 450$ ns, defined here as total coincidences, (2) -9 ns

61 014303-1

$\leqslant t \leqslant 9$ ns, as prompt coincidences, (3) -450 ns$\leqslant t \leqslant -20$ ns or 20 ns$\leqslant t \leqslant 450$ ns, as delayed coincidences. Based on the coincidences with the known γ rays of ^{143}Nd [19–21], many new γ rays were assigned to this nucleus. The half-life of the isomeric state was also extracted from the γ-γ-t data.

Linear polarization measurements are useful in determining the electric or magnetic character of γ radiation. By combining the results of linear polarization and angular distribution measurements, information on the multipolarity of γ radiation and hence on the spin and parity of the concerned nuclear state can be obtained.

For the angular distribution measurement, five Compton suppressed detectors were used simultaneously to accumulate singles spectra at angles of 90°, 75°, 55°, 45°, and 30° relative to the beam direction. By assuming the 108-, 525-, and 1576-keV γ rays depopulating the isomer in ^{142}Nd with a half-life of 18 μs to be isotropic [5,6], the relative detection efficiencies among the five detectors were determined at three energy points of 108, 525, and 1576 keV. The excited states in ^{142}Nd were populated in the ^{130}Te(^{18}O,$6n$)^{142}Nd reaction in the same run. The γ rays from target residual activity provided additional energy points for the relative detection efficiency normalizations, since these γ rays should also have isotropic intensity distributions. After correcting for the relative detection efficiencies at different angles and normalizing to one of the five detectors, the angular distribution coefficients, A_2/A_0 and A_4/A_0, for each interested transition, were extracted from least squares fits of the photopeak areas. While doing the angular distribution measurement, the γ-rf time distribution measurement was also carried out with the pulsed beam. With no beam present, a ^{152}Eu source was attached to the front of the target and γ-ray singles spectra were acquired. These ^{152}Eu source spectra were used to obtain energy and efficiency calibrations for each individual detector. The relative γ-ray intensities were extracted from the efficiency corrected singles spectra recorded by the detector located at 55°.

The γ-ray linear polarizations were measured at Kyushu University, where the tandem accelerator provided an 80-MeV ^{18}O beam. A segmented Ge detector placed at 90° relative to the beam direction, which simultaneously acted as a Compton scatterer and an absorber, was used as a Compton polarimeter. The segmented Ge is a planar detector of dimensions $50 \times 50 \times 20$ mm^3 which is divided into 25 segments by separating electrodes. The cathode of each segment provides an independent signal giving position information, and a common anode signal provides energy information. The concept of the segmented Ge detector is depicted in Ref. [22]. In the current measurement, the polarimeter was operated in a pair-wise mode, i.e., the prompt coincidence signals from all pairs of firing segments were recorded event by event on magnetic tapes. In the off-line data analysis the coincidence events were classified into two groups according to the orientation of the two firing segments with respect to the reaction plane. Thus, the polarization spectra were con-

structed by using the total energy deposited in the polarimeter.

The experimental polarization P_{exp} is determined from the anisotropy A of the γ radiation through the relations

$$P_{\text{exp}} = A/Q,$$

$$A = (N_{90} - N_0)/(N_{90} + N_0),$$

where N_{90} and N_0 are the photopeak intensities obtained when the two firing segments are oriented perpendicular or parallel to the reaction plane, respectively. Q represents the polarization sensitivity of the polarimeter, and is a function of the incident γ-ray energy. In ^{143,144}Nd, multipolarities of several strong γ rays with energies in a wide range, were assigned in the previous works [19–21,23]. The linear polarization values for these γ rays were deduced by fitting results of their angular distributions. The polarization sensitivity, measured at energy points corresponding to these selected γ rays, were therefore obtained from the deduced linear polarizations and measured anisotropy values. Hence the polarization sensitivity of the polarimeter was calibrated. The polarimeter worked very well, the electric and magnetic transitions were clearly separated into two groups in terms of the signs of their linear polarization values. These are given in Table I along with transition energies, relative intensities, angular distribution coefficients for the γ rays assigned to ^{143}Nd.

III. LEVEL SCHEME OF ^{143}Nd

Three gated spectra were produced for each of the γ rays assigned to ^{143}Nd, under the total, prompt, and delayed coincidence time conditions. Selected spectra are shown in Figs. 1–3. Figure 1 displays three background-subtracted γ-ray spectra in coincidence with the 1143-keV transition. Figure 1(a) is the spectrum gated by the 1143-keV γ ray with a time gate of ± 450 ns, Fig. 1(b) shows the γ rays in prompt coincidence with the 1143-keV transition, and Fig. 1(c) presents the spectrum for γ rays preceded by the 1143-keV transition by at least 20 ns. In Fig. 1(b) the protruded γ rays are in prompt coincidence with the 1143-keV gate. The time delay between the γ rays in Fig. 1(c) and the 1143-keV transition indicates the presence of an isomeric state. Based on the coincidence relationships, several weak γ rays were identified to ^{143}Nd, but they could not be placed in the level scheme due to their weak populations. In Fig. 1, these weak γ rays are not labeled. It is found that no γ ray crosses the isomer, which thus separates the level scheme into two parts. For the two groups of γ rays separated by the isomer, the orderings of the transitions in the level scheme are fixed either with the help of some crossover transitions or from the consideration of intensity balance in the gated spectra. Based on the analysis of the γ-γ coincidence spectra, a new level scheme of ^{143}Nd is proposed as shown in Fig. 4. Eight new γ rays of 145, 162, 423, 437, 482, 978, 1165, and 1525 keV are added into the level scheme below the 6697-keV state. The high-lying portion of the present level scheme above the 6697-keV state, which includes 32 γ rays and extends to

TABLE I. Properties of the γ rays of ^{143}Nd, produced in the ^{130}Te(^{18}O,$5n$)^{143}Nd reaction. Uncertainties are given in parentheses.

E_γ(keV) [a]	I_γ [b]	A_2/A_0	A_4/A_0	Pola.	$E_i \rightarrow E_f$	$J_i \rightarrow J_f$
61.0					3085→3024	$23/2^+ \rightarrow 21/2^+$
91.6	18.1(18)				2490→2398	$19/2^- \rightarrow 17/2^-$
139.3	6.8(23) [d]				10669→10530	
145.0	1.6(9) [d]				3334→3189	
161.5	2.5(10) [d]				4225→4063	$27/2^+ \rightarrow$
173.7	38.1(1.3)	−0.18(4)	0.03(4)	−0.28(6)	3085→2911	$23/2^+ \rightarrow 21/2^+$
178.2	3.0(8) [d]				5000→4822	$31/2^+ \rightarrow$
179.6	2.2(7) [d]				9168→8989	$\rightarrow 49/2^+$
193.4	3.4(14) [d]				6697→6503	$39/2^- \rightarrow$
206.4	1.1(7) [d]				6697→6491	$39/2^- \rightarrow$
214.5	21.9(21)	−0.21(4)	0.04(5)	−0.38(9)	5345→5130	$33/2^+ \rightarrow 31/2^+$
223.5	3.3(8)	−0.13(8)	0.04(5)	−0.37(10)	5507→5283	$33/2^+ \rightarrow 31/2^+$
230.7	2.0(10) [d]				11789→11558	
246.4	7.0(8)				6239→5992	$\rightarrow 35/2^-$
292.8	4.7(7)	−0.25(10)	0.11(3)	−0.10(14)	5000→4707	$31/2^+ \rightarrow$
299.2	8.0(8) [d]	−0.25(5)	0.00(6)	−0.19(11)	4524→4225	$29/2^+ \rightarrow 27/2^+$
300.6	1.8(6) [d]				8989→8689	$49/2^+ \rightarrow$
321.6	2.4(11) [d]				11789→11467	
323.5	3.1(14) [d]	−0.30(9)	0.14(10)	−0.12(13)	6239→5915	$\rightarrow 35/2^-$
338.6	14.4(6)	−0.23(2)	0.12(5)	0.31(5)	8989→8651	$49/2^+ \rightarrow 47/2^-$
344.4	3.7(5)	−0.21(5)	0.06(7)	−0.34(11)	5345→5000	$33/2^+ \rightarrow 31/2^+$
364.5	10.4(10)	−0.13(8)	0.06(5)	−0.33(7)	5000→4635	$31/2^+ \rightarrow 29/2^+$
372.5	35.3(23)	−0.15(4)	0.00(2)	−0.34(8)	3458→3085	$25/2^+ \rightarrow 23/2^+$
379.3	63.7(27)	−0.12(6)	0.05(6)	−0.28(5)	2398→2019	$17/2^- \rightarrow 15/2^-$
398.3	5.0(9)				10530→10132	$\rightarrow 53/2^+$
407.5	3.1(6)	−0.11(5)	−0.01(5)	0.30(8)	5915→5507	$35/2^- \rightarrow 33/2^+$
410.3	16.2(9)	−0.12(7)	0.02(5)	−0.37(7)	4635→4225	$29/2^+ \rightarrow 27/2^+$
420.8	48.0(12)	−0.16(3)	0.00(3)	0.29(5)	2911→2490	$21/1^+ \rightarrow 19/2^-$
423.0	3.4(11) [d]				5130→4707	$31/2^+ \rightarrow$
427.7	9.2(17)	0.18(4)	0.03(3)	−0.35(10)	5428→5000	$33/2^+ \rightarrow 31/2^+$
436.7	2.7(8) [d]				3189→2752	$\rightarrow 17/2^+$
445.9	3.6(14)	−0.19(9)	0.08(8)	0.28(12)	6239→5793	
448.0 [c]	15.0(30)				4524→4076	$29/2^+ \rightarrow 27/2^+$
456.1	3.0(14) [d]				4076→3620	$27/2^+ \rightarrow$
481.9	1.9(10) [d]				4707→4225	$\rightarrow 27/2^+$
484.7	3.2(12) [d]				5992→5507	$35/2^- \rightarrow 33/2^+$
486.7	2.7(11) [d]				5915→5428	$35/2^- \rightarrow 33/2^+$
494.4	23.3(28)	−0.10(4)	−0.03(4)	−0.29(12)	5130→4635	$31/2^+ \rightarrow 29/2^+$
503.2	1.9(5) [d]				7021→6518	
526.2	9.1(19)				6518→5992	$\rightarrow 35/2^-$
534.1	15.2(12)	−0.10(5)	0.05(6)	0.28(6)	3024→2490	$21/2^+ \rightarrow 19/2^-$
537.7	6.6(10)				10669→10132	$\rightarrow 53/2^+$
550.0	2.6(9) [d]				6057→5507	$\rightarrow 33/2^+$
563.8	9.0(18)	−0.16(5)	0.04(5)	0.36(9)	5992→5428	$35/2^- \rightarrow 33/2^+$
570.1	23.1(21)	−0.22(10)	0.00(8)	0.23(10)	5915→5345	$35/2^- \rightarrow 33/2^+$
575.8	4.0(16)	−0.19(6)	0.11(12)	0.30(8)	6491→5915	$\rightarrow 35/2^-$
587.8	6.3(24)				6826→6239	
593.4	1.3(4) [d]				7891→7297	
618.7	9.0(30) [d]				4076→3458	$27/2^+ \rightarrow 25/2^+$
623.9	5.0(7)				10756→10132	$\rightarrow 53/2^+$
639.7	1.4(6) [d]				6697→6057	$39/2^- \rightarrow$
647.2	7.8(11)	−0.23(8)	0.09(10)	0.44(10)	5992→5345	$35/2^- \rightarrow 33/2^+$

TABLE I. (*Continued*).

E_γ(keV) [a]	I_γ [b]	A_2/A_0	A_4/A_0	Pola.	$E_i \rightarrow E_f$	$J_i \rightarrow J_f$
673.3	1.5(7) [d]				$7969 \rightarrow 7296$	
681.9	1.8(5) [d]				$8651 \rightarrow 7969$	$47/2^- \rightarrow$
709.1	7.7(16)				$5345 \rightarrow 4635$	$33/2^+ \rightarrow 29/2^+$
711.8	3.0(8) [d]				$11467 \rightarrow 10756$	
759.7	7.2(13)	$-0.21(5)$	0.14(11)	$-0.35(9)$	$8651 \rightarrow 7891$	$47/2^- \rightarrow$
767.4	1.0(5) [d]				$4225 \rightarrow 3458$	$27/2^+ \rightarrow 25/2^+$
771.1	5.5(19) [d]				$12560 \rightarrow 11789$	
774.7	2.0(8) [d]				$5000 \rightarrow 4225$	$31/2^+ \rightarrow 27/2^+$
781.4	1.1(5) [d]				$7021 \rightarrow 6239$	
782.2	7.3(12)	0.22(8)	$-0.28(27)$	0.49(13)	$6697 \rightarrow 5915$	$39/2^- \rightarrow 35/2^-$
791.0	78.0(31)	$-0.25(4)$	0.06(7)	0.34(12)	$2019 \rightarrow 1228$	$15/2^- \rightarrow 13/2^+$
793.8	1.6(7) [d]				$7297 \rightarrow 6503$	
798.0	6.7(14) [d]				$11467 \rightarrow 10669$	
801.7	4.9(10) [d]				$8651 \rightarrow 7849$	$47/2^- \rightarrow 43/2^-$
804.9	3.2(13)				$7296 \rightarrow 6491$	
833.5	3.0(13)				$7531 \rightarrow 6697$	$43/2^- \rightarrow 39/2^-$
838.7	1.6(7) [d]				$8689 \rightarrow 7849$	$\rightarrow 43/2^-$
869.8	3.4(12) [d]				$7891 \rightarrow 7021$	
888.8	3.2(10) [d]				$11558 \rightarrow 10669$	
963.4	2.4(7) [d]				$10132 \rightarrow 9168$	$53/2^+ \rightarrow$
978.3	2.1(8) [d]				$4063 \rightarrow 3085$	$\rightarrow 23/2^+$
982.7	8.4(17)	0.34(12)	0.20(20)	0.37(14)	$5507 \rightarrow 4524$	$33/2^+ \rightarrow 29/2^+$
1064.7	4.0(15) [d]				$7891 \rightarrow 6826$	
1120.2	1.3(6) [d]				$8651 \rightarrow 7531$	$47/2^- \rightarrow 43/2^-$
1129.4	3.7(11)				$3620 \rightarrow 2490$	$\rightarrow 19/2^-$
1139.8	26.4(13)	0.34(8)	$-0.05(4)$	0.45(9)	$4225 \rightarrow 3085$	$27/2^+ \rightarrow 23/2^+$
1143.4	15.3(22)	0.33(8)	0.02(6)	0.32(8)	$10132 \rightarrow 8989$	$53/2^+ \rightarrow 49/2^+$
1152.0	5.8(17)	0.13(8)	0.08(11)	0.41(10)	$7849 \rightarrow 6697$	$43/2^- \rightarrow 39/2^-$
1158.5	3.4(14)				$6503 \rightarrow 5345$	$\rightarrow 33/2^+$
1164.9	1.4(6) [d]				$4076 \rightarrow 2911$	$27/2^+ \rightarrow 21/2^+$
1177.0	15.1(23)	0.36(10)	$-0.07(8)$	0.35(11)	$4635 \rightarrow 3458$	$29/2^+ \rightarrow 25/2^+$
1193.2	2.7(8)				$7891 \rightarrow 6697$	$\rightarrow 39/2^-$
1207.0	3.2(8)	0.35(17)	$-0.15(13)$	0.45(13)	$5283 \rightarrow 4076$	$31/2^+ \rightarrow 27/2^+$
1228.2	100(29)	0.40(5)	$-0.08(8)$	0.50(8)	$1228 \rightarrow 0$	$13/2^+ \rightarrow 7/2^-$
1249.4	6.8(16)	0.37(13)	$-0.14(15)$	0.34(11)	$4707 \rightarrow 3458$	$\rightarrow 25/2^+$
1364.2	5.3(20)				$4822 \rightarrow 3458$	$\rightarrow 25/2^+$
1524.9	5.0(18)	0.35(3)	$-0.05(5)$	0.40(10)	$2752 \rightarrow 1228$	$17/2^+ \rightarrow 13/2^+$

[a]Energies obtained from single and coincidence measurements, accurate to ± 0.5 keV.

[b]γ-ray intensities relative to the 1228-keV γ-ray intensity.

[c]Double line in ^{143}Nd.

[d]Estimated from coincidence data.

12 560 keV in excitation energy, is completely different from those proposed in the previous works [4,19–21].

Fortunately, all the strong γ rays below the isomer show an apparent angular distribution effect, in other words, the angular distributions are anisotropic for the γ rays depopulating the isomer. The above observation indicates that the alignment of the isomer spin, which was caused by the nuclear reaction, was not completely destroyed by paramagnetic relaxation effect during the isomer's lifetime [15]. This enables the multipolarities of the γ rays to be determined by combining the results of the angular distribution and linear polarization measurements. The results listed in Table I al-

low straightforward determinations of spins and parities for the yrast and several non-yrast states in ^{143}Nd. Some brief explanations of the level scheme are given below.

Figure 2 shows the summation of two spectra gated on the 1525- and 437-keV peaks, respectively. Only the cascade consisting of the 1525-, 437-, and 145-keV transitions are in coincidence with the 1228-keV γ ray. Therefore, this cascade is proposed to build directly on the first excited state at 1228 keV. The order of these transitions is determined from the relative intensities in the coincidence spectra. From the results of the γ-ray angular distribution and linear polarization measurements, an $E2$ character for the 1525-keV tran-

FIG. 1. (a) A spectrum of γ rays in coincidence with the 1143-keV γ ray within ± 450 ns. (b) Spectrum showing the γ rays in prompt coincidence with the 1143-keV transition. (c) Spectrum of γ rays preceded by the 1143-keV transition by at least 20 ns.

sition is obtained. Thus, the spin and parity of $17/2^+$ are assigned for the 2752-keV level. Additionally, the time distribution of the 1525-keV peak relative to the rf signal indicates a delayed component with a long half-life. This half-life could not be extracted due to its weak population and the improper time window used in the γ-rf time distribution measurement. Because of the high background in the low

FIG. 2. Summation of two spectra gated on the 1525- and 437-keV γ rays, respectively.

FIG. 3. Spectrum of γ rays gated on the 1165-keV transition.

energy region, it is impossible to produce reliable time distributions for the very weak 437- and 145-keV peaks. This makes it difficult to determine the isomeric position. However, it is most probable that the 3334-keV state is an isomer

FIG. 4. Level scheme of ^{143}Nd proposed in the present work.

as suggested in the following weak coupling discussion.

Up to the 5992-keV state, the present spin assignments confirm the results proposed in Refs. [4] and [21], but discrepancies for the parity assignments of two levels at 5992 and 5283 keV are found between the present and the previous works [21]. Additionally, parities are assigned in the present work to several levels below the 5992-keV state for the first time. Both the 564- and 647-keV transitions, depopulating the 5992-keV level, have $E1$ multipolarities. Both levels populated by these transitions have spin and parity values of $33/2^+$, so we could assign $J^\pi = 35/2^-$ to the 5992-keV state. However, positive parity was assigned to this state in Ref. [21]. From the $M1$ and $E2$ characters of the 299- and 983-keV transitions, spin and parity values of $29/2^+$ and $33/2^+$ are assigned to the states at 4524 and 5507 keV, respectively. The 224-keV transition depopulates the 5507-keV state and feeds the 5283 keV state. This transition is a stretched magnetic dipole, and thus allows the assignment of $J^\pi = 31/2^+$ to the state at 5283 keV. In Ref. [21], the conversion electron measurement suggested that the 224-keV transition had an $E1$ multipolarity, so negative parity was proposed for the 5283-keV state. The weak 1207-keV transition depopulating the $J^\pi = 31/2^+$ 5283-keV level shows a possible $E2$ character; thus, the spin and parity of $27/2^+$ are tentatively assigned to the 4076-keV state populated by the 1207-keV transition. The 5915-keV level is connected to the $J^\pi = 33/2^+$ 5345-keV state by the 570-keV transition, which has an $E1$ character, yielding $J^\pi = 35/2^-$ for the 5915-keV state.

The present work could not provide evidence to reverse the order of the 379- and 92-keV transitions as suggested in Ref. [21]. The 1232- and 277-keV transitions, which were put into the level scheme in Ref. [21], can indeed be assigned to ^{143}Nd, but both of them show clear coincidences with the 92- and 379-keV transitions. The spectra gated on the 1232- and 277-keV transitions are too complicated to be used to locate these two transitions into the level scheme. Instead of the 1232- and 277-keV transitions, the 1165-keV transition is proposed in the present work to be in parallel with the 1129-keV transition. Figure 3 shows the spectrum produced by gating on the 1165-keV peak. This spectrum is contaminated by the 1163-keV peak in ^{142}Nd [5,6], for example, the line just above 100 keV is the 108-keV peak in ^{142}Nd. It seems that the 1165-keV transition should be located between the 2911- and 4076-keV states according to the coincidence relationships. However, with $J^\pi = 27/2^+$ for the 4076-keV state, the 1165-keV transition would have an $M3$ character and hence its slow transition rate could not compete with other branches depopulating the 4076-keV state. Due to the doublet character of the 448- and 619-keV transitions, the spin and parity assignments of the 4076-keV state could not be checked with these independent transitions. The spin and parity values of the 4076-keV state together with the 1165-keV transition are tentatively presented in the present level scheme.

The combination of the angular distribution and linear polarization data determines the multipolarity of 782-keV γ ray, which feeds the 5915-keV state from the 6697-keV state, to be stretched $E2$. Considering the 5915-keV state
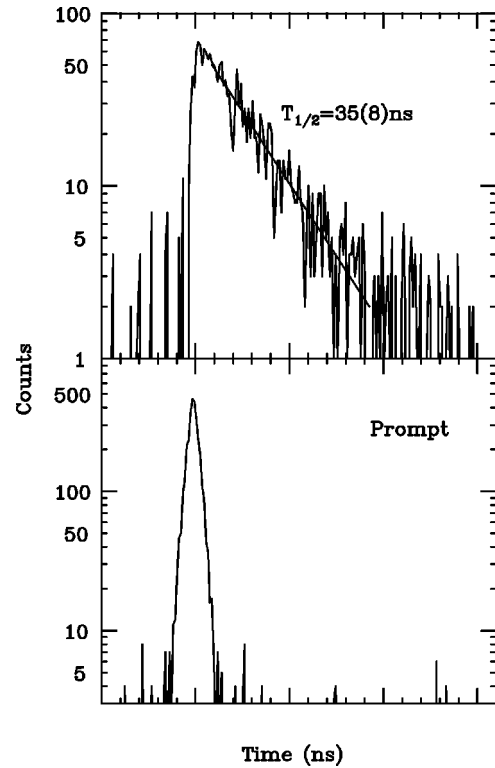
FIG. 5. (a) The time distribution between the two γ-ray groups lying above and below the isomeric state at 8989 keV and (b) the time distribution between prompt coincidence γ rays.

with $J^\pi = 35/2^-$, spin and parity of $39/2^-$ are assigned for the 6697-keV level. The present $E2$ assignment for the 782-keV γ ray is not consistent with a dipole character suggested from the DCO ratio in Ref. [4]. The 1120-, 834-, 802-, and 1152-keV transitions show $E2$ characters. From their coincidence relationships three energy levels are established at 7531-, 7849-, and 8651-keV with spin and parity values of $43/2^-$, $43/2^-$, and $47/2^-$, respectively. The 339-keV transition feeds the 8651-keV state and depopulates the 8989-keV state. Based on the analysis of the coincidence spectra obtained with different time conditions, the 8989-keV state is proposed to be an isomer. An $E1$ character is assigned to the 339-keV transition and thus $J^\pi = 49/2^+$ can be assigned to the isomer at 8989 keV.

The 13 γ rays lying above the isomer establish nine states. The 1143-keV transition shows an $E2$ character, so the spin and parity of $53/2^+$ are assigned to the 10 132-keV state. No angular distribution or linear polarization information is available for the other γ rays.

Above the 8989-keV isomer the γ rays have considerable intensities. This makes it possible to extract the half-life of the 8989-keV isomer from the γ-γ-t data. Figure 5(a) shows the time distribution between the two γ-ray groups, which lie above and below the isomeric state, respectively. The time distribution between prompt coincidence γ rays is presented in Fig. 5(b) for comparison. The latter distribution represents the time jitter of the detection system and its associated electronics. A half-life of 35 ± 8 ns was extracted for the isomer at 8989 keV from an exponential fit to the curve in Fig. 5(a).
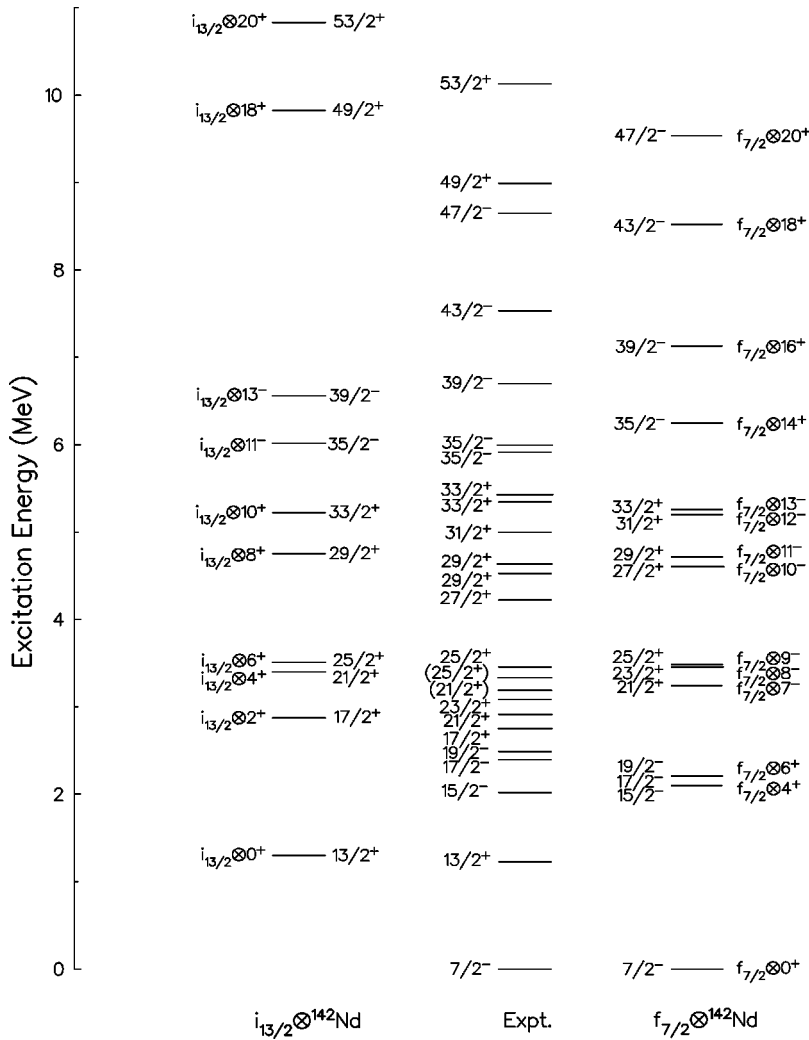
FIG. 6. Comparison of experimentally observed levels in ^{143}Nd with those calculated with the zero-order weak coupling calculation described in the text. The configurations are given in terms of the single neutron states and the ^{142}Nd core states.

IV. DISCUSSION

A. Weak coupling in ^{143}Nd

In the weak coupling framework, it would be expected that states in ^{143}Nd arise from the coupling of the valence orbits occupied by the odd neutron to states in the ^{142}Nd core nucleus. The important neutron orbits, which contribute to form yrast states, outside of the $N = 82$ closed shell are $2f_{7/2}$, $1h_{9/2}$, and $1i_{13/2}$ [4,19–21]. Previous ^{142}Nd(d,p) reaction data [24–26] suggested that the $f_{7/2}$, $h_{9/2}$, and $i_{13/2}$ single neutron orbits are located at 0, 1.4, and 1.3 MeV, respectively. Because of the high angular momentum character of the $i_{13/2}$ orbit, the coupling of the $f_{7/2}$ or $i_{13/2}$ neutron to the corresponding states in the ^{142}Nd core should compete for the yrast states in ^{143}Nd.

In the zero-order approximation it is assumed that no interaction between the valence neutron and core states exists, so the energy of a state in ^{143}Nd is calculated to be the sum of the energy of the $f_{7/2}$ or $i_{13/2}$ single neutron state and that of the corresponding state in the ^{142}Nd core [5,6]. The predictions of the weak coupling calculation, which is discussed in detail in Refs. [4,19–21], are compared with the experimental results in Fig. 6. In addition to the yrast states, a number of non-yrast states in ^{143}Nd are included in the com-

parison because they are also easily identified as corresponding to states in ^{142}Nd.

The energy spacings of the 1228-, 2752-, 3189-, and 3334-keV levels are quite similar to those of the 0^+, 2^+, 4^+, and 6^+ states in the ^{142}Nd core nucleus [5,6]. This similarity is reflected in the calculation by coupling the $i_{13/2}$ neutron to the 0^+, 2^+, 4^+, and 6^+ states in the ^{142}Nd core, as seen in Fig. 6. Because the 6^+ state in ^{142}Nd is a long-lived isomer [6], the weak coupling model would expect the 3334-keV state, which is formed by coupling the $i_{13/2}$ neutron to the 6^+ state in ^{142}Nd, to be also an isomeric state. Indeed, the time distribution of the 1525-keV peak relative to the rf signal is similar to those of the 525- and 1576-keV transitions which depopulate the 6^+ isomer in ^{142}Nd, although the statistics in the time spectrum for the 1525-keV transition are very low. This may be evidence to support the weak coupling interpretation of these states. Since no γ rays, except for that of 1228 keV, were observed in coincidence with the 145-, 437-, and 1525-keV transitions, it seems reasonable to assume the 3334-keV state is a long-lived isomer. It is this long-lived isomer that might isolate the cascade consisting of the 1525-, 437-, and 145-keV transitions. The spin and parity of $17/2^+$ determined experimentally for the 2752-keV state

are consistent with those predicted by the weak coupling calculation which also suggests spin and parity values of $21/2^+$ and $25/2^+$ for the 3189- and 3334-keV states, respectively.

The simple weak coupling calculations are generally successful in reproducing the energies of yrast states up to the $39/2^-$ yrast level in ^{143}Nd. However, the energy of the experimentally observed $27/2^+$ yrast state is much lower than the prediction of the weak coupling calculation, this problem will be discussed in the next section. Just above the $J^\pi = 39/2^-$ yrast level, the weak coupling prediction deviates significantly from the experimental observations, possibly indicating that the $N = 82$ neutron shell closure is broken above $J = 39/2$. The neutrons, which are excited across the $N = 82$ shell gap, would interact strongly with the valence neutrons so that the weak coupling picture would no longer be valid. In the following discussion, the breakdown of the $N = 82$ shell closure just above the $39/2^-$ state is clearly suggested in the deformed independent particle model calculation. It should be pointed out that the present weak coupling interpretation disagrees with that presented in Ref. [21], where a different high-lying level scheme was proposed for ^{143}Nd, and all the yrast states with spin assignments up to 43/2 were successfully reproduced with the weak coupling model.

B. Deformed independent particle model calculation

The deformed independent particle model (DIPM) described well the yrast level structure in the ^{146}Gd region [16]. The level configurations deduced from the DIPM calculations agree with the shell model assignments [27,28]. The calculations also reproduced the measured g factors and quadrupole moments of the isomers in ^{146}Gd and ^{147}Gd [16–18,29–32]. Moreover, the DIPM calculations reproduced the energy systematics of the high-lying isomers in the $N = 83$ isotones [15]. Therefore, this model could be used realistically to interpret the yrast level structure of ^{143}Nd.

The construction of model states starts with the analysis of the single particle motion in an axially symmetric potential well. For multiparticle configurations, their wave function is described by

$$\Psi = P_{N,Z}\Phi,$$

where $P_{N,Z}$ is the projector onto the space of states with neutron number N and proton number Z, and Φ is a BCS multiquasiparticle state. To each such multiparticle configuration the DIPM assigns the energy

$$E \equiv \langle H \rangle_\Psi - \widetilde{E} + E_{LD}$$

minimized with respect to the neutron and proton pairing gap parameters and the shape parameters of the single particle potential. In the above equation H denotes the independent particle plus monopole pairing force Hamiltonian. $\widetilde{E}$ is Strutinsky's smooth sum of the energies of the lowest N neutron and Z proton states [16], and E_{LD} is the sum of the surface and Coulomb energies of a liquid drop with the shape of the single particle potential. $\widetilde{E}$ and E_{LD} are func-

tions of the shape alone. A more detailed description of the model calculation is given in Ref. [16] and the references therein. In the calculation, the model states were interpreted having maximal magnetic quantum number in the direction of the nuclear symmetry axis, that is, the sum of the single-particle angular momenta of valence nucleons along the symmetry axis was taken as the total angular momentum for the concerned configuration. Figure 7 presents the comparison between the experimental and calculated level structures for ^{143}Nd. As for the excitation energy, the new $J^\pi = 49/2^+$ isomer in ^{143}Nd follows well the systematics of the high-spin isomers observed in the $N = 83$ isotones [15]. The excitation energies of these isomers are almost constant at about 8.6 MeV while the proton number changes from 65 to 60. However, the calculated excitation energies of the high-spin isomers with a set of fixed parameters, which was originally chosen to reproduce the characteristics of the high-spin isomer in ^{147}Gd [15], increase as the proton number decreases from 65 to 60 [15]. In order to achieve the best agreement between the experimental and theoretical excitation energies for the isomer in ^{143}Nd, the $Z = 64$ proton shell gap energy between the $d_{5/2}$ and $h_{11/2}$ single proton orbits was adjusted in the present calculation. The calculated excitation energy [15] for the isomer in ^{147}Gd with the set of fixed parameters was used as a reference energy to optimize the proton shell gap energy for ^{143}Nd. It is found that the most suitable proton shell gap energy for ^{143}Nd is 1.93 MeV, at which value the difference in excitation energies between the isomers in ^{147}Gd and ^{143}Nd is equal to that observed experimentally.

The DIPM reproduces the states up to the $25/2^+$ level in ^{143}Nd, although the model generally predicts higher excitation energies than those observed experimentally. The DIPM calculation suggests three quasiparticle configurations for the states lying between the $13/2^+$ and $27/2^+$ yrast states. While the $[\nu f_{7/2} \pi(d_{5/2}^{-2})]$ and $[\nu f_{7/2} \pi(d_{5/2}^{-1} g_{7/2}^{-1})]$ configurations are responsible for the negative-parity states, the positive-parity states originate from the $[\nu f_{7/2} \pi(d_{5/2}^{-1} h_{11/2})]$ and $[\nu f_{7/2} \pi(g_{7/2}^{-1} h_{11/2})]$ configurations. As presented in Fig. 7, five or seven quasiparticle configurations can be assigned to the states above the $25/2^+$ level. The DIPM calculation shows that three configurations of $[\nu f_{7/2} \pi(d_{5/2}^{-2} g_{7/2}^{-1} h_{11/2})]$, $[\nu f_{7/2} \pi(d_{5/2}^{-3} h_{11/2})]$, and $[\nu f_{7/2} \pi(d_{5/2}^{-1} g_{7/2}^{-2} h_{11/2})]$ can provide states with $J^\pi = 27/2^+$ or $29/2^+$, but the calculated excitation energies for these configurations are much too high compared with the experimental ones. The $27/2^+$ and $29/2^+$ states in ^{145}Sm were also observed experimentally at relatively low excitation energies [15]. In a recent recoil distance half-life measurements of the excited states in ^{145}Sm [33], the yrast $27/2^+$ state was found to have a half-life of 1.1 ns. The excitation energy of the $27/2^+$ state was fairly well reproduced by the shell model calculation, which indicated that the strong proton-neutron interaction involving the $h_{9/2}$ neutron lowered the excitation energy of the $27/2^+$ state in ^{145}Sm [33]. This might be a promising way to reproduce the $27/2^+$ and $29/2^+$ states in ^{143}Nd.

Along the yrast line up to $J^\pi = 39/2^-$, only the $f_{7/2}$ neutron orbit participates in the configurations. But just above the $39/2^-$ level, the DIPM calculation demonstrates that the
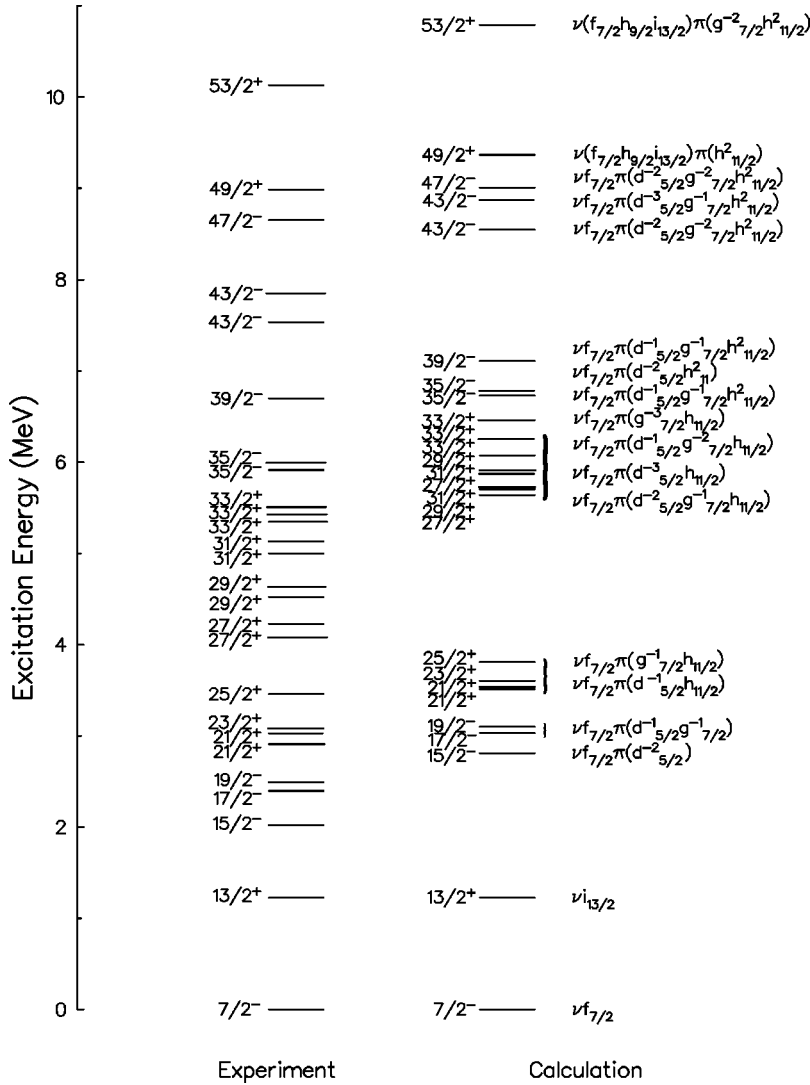
FIG. 7. Comparison between the experimentally observed levels in ^{143}Nd and those calculated by the deformed independent particle model calculation. The configurations are listed next to the corresponding calculated levels.

configurations involving three neutrons, implying neutron excitation across the $N=82$ shell gap, start to compete to become yrast states. Indeed the configuration $[\nu(d_{3/2}^{-1}f_{7/2}i_{13/2})\pi(h_{11/2}^2)]$ becomes the yrast level at spin of $41/2\hbar$. Unfortunately, no level with $J=41/2$ has been identified experimentally in the present work. Two calculated $43/2^-$ states with excitation energies at 8.55 and 8.87 MeV, have configurations of $[\nu f_{7/2}\pi(d_{5/2}^{-2}g_{7/2}^{-2}h_{11/2}^2)]$ and $[\nu f_{7/2}\pi(d_{5/2}^{-3}g_{7/2}^{-1}h_{11/2}^2)]$, respectively. While the other two $[\nu(f_{7/2}h_{9/2}i_{13/2})\pi(g_{7/2}^{-1}h_{11/2})]$ and $[\nu(f_{7/2}h_{9/2}i_{13/2})\pi(d_{5/2}^{-1}h_{11/2})]$ configurations can also provide $43/2^-$ states with comparable excitation energies at 8.92 and 8.96 MeV, respectively, these configurations involve the promotion of neutrons across the $N=82$ shell gap. Therefore, it is quite possible that the $N=82$ neutron shell closure is broken above $J=39/2$. This may be a possible reason why the weak coupling predictions deviate significantly from the experimental observations above the $39/2^-$ level.

The DIPM calculation suggests the $49/2^+$ isomer in ^{143}Nd to be a stretched configuration of $[\nu(f_{7/2}h_{9/2}i_{13/2})\pi(h_{11/2}^2)]$. This isomer was depopulated mainly by the 339-keV electric dipole transition. Based on the measured half-life of 35 ns

and the decay branching ratio for the 339-keV transition, a reduced transition probability $B(E1)$ of $1.64(0.33)\times10^{-7}$ Weisskopf units (W.u.) could be obtained for the $49/2^+ \rightarrow 47/2^- E1$ transition.

In the DIPM calculations, the nuclear deformation is restricted to purely ellipsoidal shapes and is, thus, described by the single parameter $\beta=(16\pi/5)^{1/2}(q-1)/(q+2)$ [16], where q denotes the ratio between the distance of the poles and the diameter of the equator. The calculated deformation parameters β for the yrast states in ^{143}Nd are shown in Fig. 8. For comparison, Fig. 8 also displays the calculated β values for the yrast states in ^{147}Gd as a function of spin, where three yrast isomers were identified with spin and parity values of $13/2^+$, $27/2^-$, and $49/2^+$ [17,18]. The deformation parameters, β, for the isomers in ^{147}Gd were deduced from the measured quadrupole moments [17,18], and these experimental deformation values are well reproduced by the DIPM calculation as seen in Fig. 8. The DIPM calculations show the same trend in deformation along the yrast line in ^{143}Nd and ^{147}Gd. Below the yrast $49/2^+$ isomer, the yrast states have near spherical shapes with small deformations, ranging from 0 to -0.1, but the deformation increases suddenly at
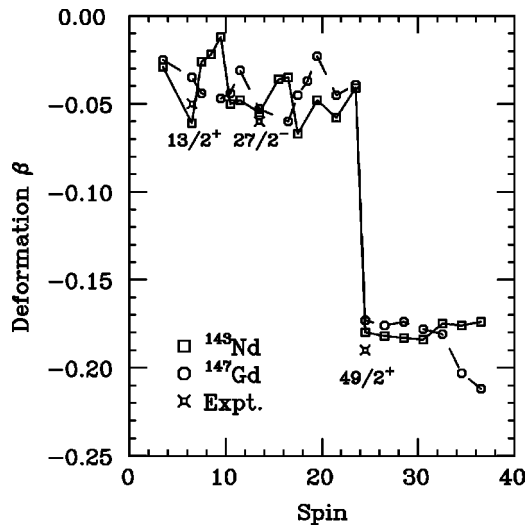
FIG. 8. The calculated deformation parameters β for the yrast states as a function of spin in ^{143}Nd and ^{147}Gd, shown by the solid and dotted lines, respectively. The experimental β values for the $13/2^+$, $27/2^-$, and $49/2^+$ isomers in ^{147}Gd are indicated by the crosses.

the $49/2^+$ isomeric position. A β value of -0.18 is obtained for the $49/2^+$ isomer in ^{143}Nd. In the $N=83$ isotones the $49/2^+$ isomers have a neutron configuration of $[(d_{3/2}^{-2})_0 f_{7/2} h_{9/2} i_{13/2}]$. The large deformation of the $49/2^+$ isomers is caused by the two $(d_{3/2}^{-2})_0$ neutron holes in this configuration, since the large quadratic term in the β depen-

dence of the $d_{3/2}$ orbit energy drives the nucleus towards a large oblate deformation [16]. As with the isomers in the heavier isotones, the occurrence of the $49/2^+$ isomer in ^{143}Nd can be interpreted as being caused by the sudden change in nuclear shape along the yrast line.

V. SUMMARY

The level scheme of ^{143}Nd has been extended up to 12 560 keV in excitation energy, including an isomer at 8989 keV with a measured half-life of 35 ± 8 ns. The spin and parity of $49/2^+$ have been assigned to the isomer in ^{143}Nd. The high-lying part of the level scheme proposed in the present work is completely different from previously published ones.

While the low-lying states in ^{143}Nd can be reproduced by the weak coupling of an $f_{7/2}$ or $i_{13/2}$ neutron to the states in the ^{142}Nd core nucleus, the breakdown of the simple weak coupling prediction has been observed above the state with $J^\pi = 39/2^-$. This might indicate that the $N=82$ neutron shell closure was broken, and neutrons below the $N=82$ shell were promoted across the shell gap to participate in generating angular moments above the state with $J^\pi = 39/2^-$.

The DIPM calculation can reproduce the yrast states in ^{143}Nd, but the predicted excitation energies are generally higher than those observed experimentally. The DIPM calculation has suggested the $49/2^+$ isomer in ^{143}Nd to be of a stretched configuration $[\nu(f_{7/2} h_{9/2} i_{13/2})\pi(h_{11/2}^2)]$, which induces a sudden increase in nuclear deformation along the yrast line, and may cause the isomerism.

[1] M. Piiparinen, Y. Nagai, P. Kleinheinz, M.C. Bosca, B. Rubio, M. Lach, and J. Blomquist, Z. Phys. A **338**, 417 (1991).

[2] T. Glasmacher, D.D. Caussyn, P.D. Cottle, T.D. Johnson, K.W. Kemper, and P.C. Womble, Phys. Rev. C **45**, 1619 (1992).

[3] X.H. Zhou, E. Ideguchi, Y. Gono, T. Kishida, S. Mitarai, T. Morikawa, H. Tsuchida, M. Shibata, H. Watanabe, M. Miyake, A. Odahara, M. Oshima, Y. Hatsukawa, S. Hamada, H. Iimura, M. Shibata, T. Ishii, and M. Ishihara, Z. Phys. A **358**, 285 (1997).

[4] O.J. Tekyi-Mensah, P.D. Cottle, J. Doring, P.V. Green, J.W. Holcomb, G.D. Johns, J.L. Johnson, T.D. Johnson, K.W. Kemper, P.L. Kerr, S.L. Tabor, P.C. Womble, and V.A. Wood, Phys. Rev. C **50**, R1759 (1994).

[5] H. Prade, J. Doring, W. Enghardt, L. Funke, and L. Kaubler, Z. Phys. A **328**, 501 (1987).

[6] R. Wirowski, J. Yan, A. Dewald, A. Gelberg, W. Lieberz, K.P. Schmittgen, A. von der Werth, and P. von Brentano, Z. Phys. A **329**, 509 (1988).

[7] S. Andre, C. Foin, V. Barci, D. Barneoud, J. Genevey, and A. Gizon, Z. Phys. A **337**, 349 (1990).

[8] J. Mcneill, R. Broda, Y.H. Chung, P.J. Daly, Z.W. Grabowski, H. Helppi, M. Kortelahti, R.V.F. Janssens, T.L. Khoo, R.D. Lawson, D.C. Radford, and J. Blomqvist, Z. Phys. A **325**, 27 (1986).

[9] J. Pedersen, B.B. Back, F.M. Bernthal, S. Bjornholm, J. Borggreen, O. Christensen, F. Folkmann, B. Herskind, T.L. Khoo, M. Neiman, F. Puhlhofer, and G. Sletten, Phys. Rev. Lett. **39**, 990 (1977).

[10] D.C.J.M. Hageman, M.J.A. de Voigt, and J.F.W. Jansen, Phys. Lett. **84B**, 301 (1979).

[11] J. Borggreen, S. Bjornholm, O. Christensen, A. Del Zoppo, B. Herskind, J. Pedersen, G. Sletten, F. Folkmann, and R.S. Simon, Z. Phys. A **294**, 113 (1980).

[12] A. Ferragut, Y. Gono, T. Murakami, T. Morikawa, Y.H. Zhang, K. Morita, A. Yoshida, M. Oshima, H. Kusakari, M. Sugawara, M. Ogawa, M. Nakajima, S. Mitarai, A. Odahara, E. Ideguchi, T. Shizuma, M. Kidera, J.C. Kim, S.J. Chae, B.J. Min, and H. Kumagai, J. Phys. Soc. Jpn. **62**, 3343 (1993).

[13] T. Murakami, Y. Gono, A. Ferragut, Y.H. Zhang, K. Morita, A. Yoshida, M. Ogawa, M. Nakajima, B.J. Min, H. Kumagai, M. Oshima, T. Morikawa, M. Sugawara, and H. Kusakai, Z. Phys. A **350**, 123 (1993).

[14] E. Ideguchi, Y. Gono, S. Mitarai, T. Morikawa, A. Odahara, M. Kidera, M. Shibata, H. Tsuchida, K. Miyazaki, M. Oshima, Y. Hatsukawa, S. Hamada, H. Iimura, M. Shibata, T. Ishii, T. Murakami, H. Kusakari, M. Sugawara, T. Kishida, K. Morita, H. Kumagai, and M. Ishihara, Z. Phys. A **352**, 363 (1995).

[15] A. Odahara, Y. Gono, S. Mitarai, T. Morikawa, T. Shizuma, M. Kidera, M. Shibata, T. Kishida, E. Ideguchi, K. Morita, A.

Yoshida, H. Kumagai, Y.H. Zhang, A. Ferragut, T. Murakami, M. Oshima, H. Iimura, M. Shibata, S. Hamada, H. Kusakari, M. Sugawara, M. Ogawa, M. Nakajima, B.J. Min, J.C. Kim, S.J. Chae, and H. Sagawa, Nucl. Phys. **A620**, 363 (1997).

[16] T. Dossing, K. Neergard, and H. Sagawa, Phys. Scr. **24**, 258 (1981).

[17] O. Hausser, H.E. Mahnke, T.K. Alexander, H.R. Andrews, J.F. Sharpey-Schafer, M.L. Swanson, D. Ward, P. Taras, and J. Keinonen, Nucl. Phys. **A379**, 287 (1982).

[18] E. Dafni, J. Bendahan, C. Broude, G. Goldring, M. Hass, E. Naim, M.H. Rafailovich, C. Chasman, O.C. Kistner, and S. Vajda, Nucl. Phys. **A443**, 135 (1985).

[19] S.M. Aziz, P.D. Cottle, K.W. Kemper, M.L. Owens, and S.L. Tabor, Phys. Rev. C **41**, 1268 (1990).

[20] D.D. Caussyn, S.M. Aziz, P.D. Cottle, T. Glasmacher, and K.W. Kemper, Phys. Rev. C **43**, 2098 (1991).

[21] M. Fauerbach, L.A. Riley, P.D. Cottle, R.A. Kaye, and K.W. Kemper, Phys. Rev. C **58**, 826 (1998).

[22] Y. Gono, T. Morikawa, T. Kishida, K. Morita, A. Odahara, E. Ideguchi, T. Murakami, M. Oshima, M. Sugawara, H. Kusakari, H. Kumagai, H. Tsuchida, M. Ogawa, M. Kidera, M. Shibata, K. Miyazaki, S. Mitarai, Y.H. Zhang, A. Ferragut, G.H. Liu, Y. Hatsukawa, J.C. Kim, S.A. Shin, and M. Ishihara, Nucl. Phys. **A588**, 241c (1995).

[23] J.K. Jewell, O.J. Tekyi-Mensah, P.D. Cottle, J. Doring, P.V. Green, J.W. Holcomb, G.D. Johns, J.L. Johnson, T.D. Johnson, K.W. Kemper, P.L. Kerr, S.L. Tabor, P.C. Womble, and V.A. Wood, Z. Phys. A **348**, 69 (1994).

[24] W. Booth, S. Wilson, and S.S. Ipson, Nucl. Phys. **A238**, 301 (1975).

[25] J.C. Veefkind, D. Spaargaren, J. Bolk, and K. Heyde, Z. Phys. A **275**, 55 (1975).

[26] L.K. Peker, Nucl. Data Sheets **64**, 429 (1991).

[27] P. Kleinheinz, Report No. ANL-PHY-79-4, 1979 (unpublished), p. 125.

[28] B. Hass, H.R. Andrews, O. Hausser, D. Horn, J.F. Sharpey-Schafer, P. Taras, W. Trautmann, D. Ward, T.L. Khoo, and R.K. Smither, Phys. Lett. **84B**, 178 (1979).

[29] R. Broda, P. Kleinheinz, S. Lunardi, J. Styczen, and J. Blomqvist, Z. Phys. A **305**, 281 (1982).

[30] O. Bakander, C. Baktash, J. Borggreen, J.B. Jensen, K. Kownacki, J. Pedersen, G. Sletten, D. Ward, H.R. Andrews, O. Hausser, P. Skensved, and P. Taras, Nucl. Phys. **A389**, 93 (1982).

[31] O. Hausser, P. Taras, W. Trautmann, D. Ward, T.K. Alexander, H.R. Andrews, B. Hass, and D. Horn, Phys. Rev. Lett. **42**, 1451 (1979).

[32] M.W. Drigert, M. Piiparinen, R.V.F. Janssens, R. Holzmann, I. Ahmad, J. Borggreen, R.R. Chasman, P.J. Daly, B.K. Dichter, H. Emling, U. Garg, Z.W. Grabowski, T.L. Khoo, W.C. Ma, M. Quader, D.C. Radford, and W. Trzaska, Nucl. Phys. **A515**, 466 (1990).

[33] A. M. El-Badry, T. Kuroyanagi, S. Mitarai, A. Odahara, Y. Gono, S. Morinobu, and K. Ogawa, Eur. Phys. J. A **3**, 133 (1998).